CHINA FOUNDRY Research & Development
Vol. 20 No. 1 January 2023
www.springer.com/41230
https://doi.org/10.1007/s41230-022-2082-2

Effects of magnesium and copper additions on tensile properties of Al-Si-Cr die casting alloy under as-cast and T5 conditions

***Hong-yi Zhan[1], Yi-wu Xu[2, 3], Pan Wang[1], Jian-feng Wang[1], Jin-ping Li[4], and Le-peng Zhang[4]**

1. General Motors Global Research & Development, China Science Laboratory, Shanghai 201206, China

2. School of Materials Science and Engineering, Shanghai Jiao Tong University, Shanghai 200240, China

3. General Motors (China) Investment Co., Ltd., Shanghai 201206, China

4. China International Intellectech Corporation (CIIC), Beijing 100004, China

Abstract: Aluminum high pressure die casting (HPDC) technology has evolved in the past decades, enabling stronger and larger one-piece casting with significant part consolidation. It also offers a higher design freedom for more mass-efficient thin-walled body structures. For body structures that require excellent ductility and fracture toughness to be joined with steel sheet via self-piercing riveting (for instance, shock towers and hinge pillars, etc.), a costly T7 heat treatment comprising a solution heat treatment at elevated temperatures (450 °C–500 °C) followed by an over-ageing heat treatment is needed to optimize microstructure for meeting product requirement. To enable cost-efficient mass production of HPDC body structures, it is important to eliminate the expensive T7 heat treatment without sacrificing mechanical properties. Optimizing die cast alloy chemistry is a potential solution to improve fracture toughness and ductility of the HPDC components. The present study intends to tailor the Mg and Cu additions for a new Al-Si-Cr type die casting alloy (registered as A379 with The Aluminum Association, USA) to achieve the desired tensile properties without using T7 heat treatment. It was found that Cu addition should be avoided, as it is not effective in enhancing strength while degrades tensile ductility. Mg addition is very effective in improving strength and has minor impact on tensile ductility. The investigated Al-Si-Cr alloy with a nominal composition of Al-8.5wt.%Si-0.3wt.%Cr-0.2wt.%Fe shows comparable tensile properties with the T7 treated AlSi10MnMg alloy which is currently used for manufacturing shock towers and hinge pillars.

Keywords: Al-Si alloy; intermetallics; high pressure die casting; tensile property; T7 heat treatment

CLC numbers: TG146.21 **Document code:** A **Article ID:** 1672-6421(2023)01-012-11

1 Introduction

Applying aluminum (Al) alloys to substitute mild steel is one of the most effective approaches to lighten the body, chassis, and powertrain components for improving automotive fuel economy. Aluminum casting components account for over 70% in the total mass of Al-made components in passenger vehicles [1]. Among various casting methods, high pressure die casting (HPDC) is suitable for manufacturing thin-walled components with precise dimension [2]. In addition, HPDC is productive and cost-efficient for mass production (~1,000,000 to 2,000,000 parts in life cycle) [3]. Taking advantages of good melt fluidity of Al alloys, HPDC can contribute to multi-part consolidation and stiffness improvement via smart design. In the past decade, due to the development of low-Fe hypoeutectic Al-Si die cast alloys (Al-Si-Mg-Mn system, e.g., SF36 and Aural-2) [3] and super-vacuum HPDC technology [4], more and more body structures such as shock towers, hinge pillars, cross members and longitudinal rails, which require excellent rivetability and crashworthiness, have been manufactured by HPDC [5,6].

In the current production of high integrity HPDC body structures which require excellent rivetability with steel sheet and crashworthiness, a complicated heat treatment recipe, also known as T7 heat treatment, comprising a solution heat treatment conducted at elevated temperatures (450 °C to 500 °C) followed by an over-ageing heat treatment is needed to modify the casting microstructure [4,7,8]. The most common HPDC component requiring T7 heat treatment is shock tower [5]. However, T7 heat treatment induces extra cost. Previous cost calculation study has shown that eliminating

***Hong-yi Zhan**

Male, born in 1990, Ph.D., Senior Researcher. Research interests: casting of light metals. To date, he has published 20 technical papers.

E-mail: henry.zhan@gm.com

Authors Hong-yi Zhan and Yi-wu Xu contributed equally to this article.

Received: 2022-06-13; Accepted: 2022-08-03

T7 heat treatment is vital to make the mass production of Al HPDC body structures cost-efficient [3]. Moreover, for large one-piece body structures, solution heat treatment is not applicable as even fan cooling from elevated temperatures may induce excessive distortion of the thin-walled structures. Therefore, large one-piece body structures can only be assembled under as-cast (AC), paint baked or T5 (artificial ageing heat treatment following shape casting) conditions. Therefore, it is important to investigate means to eliminate T7 heat treatment while maintaining desired mechanical properties for HPDC components. Optimizing die cast alloy chemistry is a promising solution for improving mechanical properties.

In a newly developed Al-Si-Cr die cast alloy system, a certain amount of Cr is added in lieu of Mn and Fe to resolve the die-soldering issue [9]. The Al-Si-Cr die casting alloy has been proven to have excellent combination of strength and ductility in the as-cast state [10,11], and it may be a promising candidate alloy to achieve excellent ductility and fracture toughness without applying T7 heat treatment. Magnesium (Mg) and copper (Cu) are two of the mostly common elements added to Al-Si based casting alloys for enhancing strength [12-16]. Their additions need to be tuned for the Al-Si-Cr alloy to achieve optimum mechanical properties. In the present study, effects of Mg and Cu additions on the tensile properties of Al-Si-Cr die cast alloy under as-cast and T5 conditions were investigated. Optical microscopy (OM) and scanning electron microscopy (SEM) were applied to characterize microstructures for understanding the relationship between microstructure and tensile properties. In addition, T7 heat treated AlSi10MnMg alloy, which is often used in the current casting of body structures [3], was prepared along with the Al-Si-Cr alloy samples as the baseline for comparison purpose.

2 Experimental procedures

2.1 Casting process and heat treatments

Table 1 lists the nominal chemical compositions of the alloys prepared in the present study and the corresponding actual chemical compositions measured by a spark optical emission spectrometer (Spark-OES). A LK DCC400 cold chamber die casting machine with a locking force of ~400 t was employed to produce 30 castings for each composition. During the casting process, melt temperature in the holding furnace was controlled at 700±5 °C for Al-Si-Cr alloys and 690±5 °C for AlSi10MnMg alloy. Key processing parameters including slow shot speed, fast shot speed and intensification pressure were set according to the supplier's suggestion. During the casting process, mold temperature was controlled at 150±10 °C. After one casting cycle was completed, product was extracted and immediately quenched in water which was kept at a temperature of about 30 °C. Figures 1(a) and (b) show the schematics of the casting coupon and the actual casting produced, respectively. Extraction locations for tensile testing sample are indicated by the dotted line box in Fig. 1(a), and the corresponding sample dimension is shown in Fig. 1(c). The selection of sampling location is based on the supplier's experience, i.e., the locations with minimal casting defect.

The selected cast-to-size bars were cut off from the obtained castings and deburred. Heat treatments were conducted in an electrically heated air-circulating chamber furnace with temperature variation of less than 5 °C. Heat treatment recipes applied in the present study include two T5 recipes and one T7 recipe, as summarized in Table 2. The T51 schedule was carried out at 180 °C for 45 min to simulate typical automotive paint baking process. The T52 process was carried out at 205 °C for 60 min to achieve a more stabilized strength. For T7 treated

Table 1: Nominal chemical compositions and experimentally measured compositions of the alloys prepared (wt.%)

Alloy designation		Si	Mg	Fe	Mn	Cr	Cu	Ti	Sr (ppm)	Al
AlSiCr	Nominal	7.5–8.5	<0.01	<0.25	<0.01	0.25–0.30	<0.05	0.05–0.1	50–160	Bal.
	Actual	8.63	0.00	0.19	0.00	0.31	0.00	0.05	87	Bal.
AlSiCr0.2Mg	Nominal	7.5–8.5	0.15–0.25	<0.25	<0.01	0.25–0.30	<0.05	0.05–0.1	50–160	Bal.
	Actual	8.50	0.25	0.19	0.00	0.31	0.02	0.05	89	Bal.
AlSiCr0.3Mg	Nominal	7.5–8.5	0.30–0.40	<0.25	<0.01	0.25–0.30	<0.05	0.05–0.1	50–160	Bal.
	Actual	8.40	0.39	0.19	0.00	0.31	0.02	0.05	86	Bal.
AlSiCr0.5Cu	Nominal	7.5–8.5	<0.01	<0.25	<0.01	0.25–0.30	0.45-0.55	0.05–0.1	50–160	Bal.
	Actual	8.55	0.00	0.19	0.00	0.32	0.51	0.08	42	Bal.
AlSiCr0.5Cu0.2Mg	Nominal	7.5–8.5	0.15–0.25	<0.25	<0.01	0.25–0.30	0.45–0.55	0.05–0.1	50–160	Bal.
	Actual	8.49	0.22	0.18	0.00	0.32	0.51	0.08	43	Bal.
AlSi10MnMg	Nominal	9.5–11.5	0.27–0.33	<0.20	0.45–0.55	/	<0.01	0.05–0.1	100–160	Bal.
	Actual	11.2	0.31	0.18	0.45	/	0.00	0.00	120	Bal.

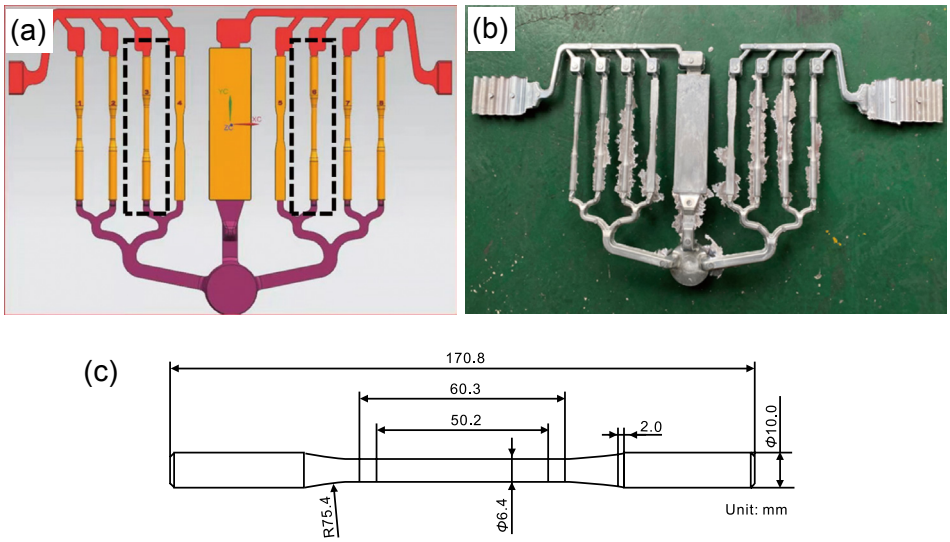

Fig. 1: Schematics of coupon (a) and actual (b) castings made by HPDC, and detailed dimension of the tensile bars (c) extracted from the dotted line boxes in (a)

Table 2: A summary of alloys and their corresponding heat treatment processes

Alloy	State	
AlSiCr	AC	As-cast
AlSiCr0.2Mg	AC	As-cast
	T51	180 °C×45 min
	T52	205 °C×60 min
AlSiCr0.3Mg	AC	As-cast
	T51	180 °C×45 min
	T52	205 °C×60 min
AlSiCr0.5Cu	AC	As-cast
	T51	180 °C×45 min
	T52	205 °C×60 min
AlSiCr0.2Mg0.5Cu	AC	As-cast
	T51	180 °C×45 min
	T52	205 °C×60 min
AlSi10MnMg	AC	As-cast
	T7	460 °C×60 min + fan cooling + 230 °C×180 min

samples, solution heat treatment was carried out at 460 °C for 60 min followed by fan cooling. Then, an over-ageing heat treatment was done at 230 °C for 3 h immediately following the solution treatment.

2.2 Microstructural characterization and hardness testing

Specimens for cross-section macrostructural/microstructural observation were cut about 15 mm from the fractured surface (Line A), as illurstrated in Fig. 2. The sections were all firstly wet ground using silicon carbide papers, then mechanically polished and ultrasonically cleaned. The as-polished cross-section microstructure of the nine tested tensile samples are shown in Fig. 2. It can be seen that the area fraction of casting defects such as gas pores and shinkage pores are limited, which is beneficial for reducing ductility variations caused by such casting defects. Specimens for OM observation were etched using the Keller's reagent (1% hydrofluoric acid, 2.5% nitric acid, 1.5% hydrochloric acid and 95% distilled water). SEM observation including EDS was performed on a Carl Zeiss AURIGA instrument equipped with the Oxford EDX system. Tensile tests were carried out using a INSTRON 5982 tensile frame at room temperatures with an initial strain rate of ~1×10^{-3} s^{-1}. Averaged tensile property data for each alloy and heat treatment condition were calculated from at least 5 tested samples free of visible defects on their fractured surfaces.

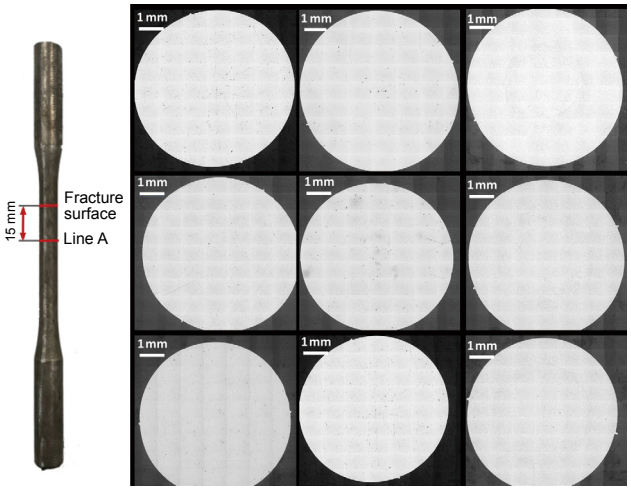

Fig. 2: Configuration of sampling location (Line A) for cross-section macrostructural/microstructural characterization (left), and some as-polished cross-sections (right), indicating good casting quality

3 Results and discussion

3.1 Effects of Mg addition on tensile properties and microstructures

Table 3 lists the averaged tensile properties of the alloys. Tensile curves for Mg-free and Mg-added Al-Si-Cr die casting alloys in the as-cast state and T5 heat treated states are shown in Figs. 3(a) and (b), respectively. Figures 4(a) and (b) were plotted based on averaged 0.2% proof stress ($R_{P0.2}$), averaged ultimate tensile stress (UTS) and averaged elongation at fracture (EL) listed in Table 3, to show effects of Mg addition and T5 heat treatment on tensile properties. The Mg-free alloy shows superior ductility with an averaged EL higher than 15% whereas its averaged $R_{P0.2}$ is below 120 MPa. Both $R_{P0.2}$ and UTS of the alloys increase with increasing Mg levels. Under the as-cast condition, 0.25wt.% Mg addition leads to about 12% increment in both $R_{P0.2}$ and UTS, while 0.39wt.% Mg addition leads to about 27% and 18% increment in $R_{P0.2}$ and UTS. Furthermore, it is interesting to note that the remarkable strength improvement in the as-cast AlSiCr0.3Mg alloy is not accompanied with any significant loss in ductility. According to Fig. 4(a), T5 heat treatment significantly enhances $R_{P0.2}$ for the AlSiCr0.2Mg and AlSiCr0.3Mg alloys. After solidification, Mg and Si are, to some extent, supersaturated in the α-Al grains in the AlSiCr0.2Mg and AlSiCr0.3Mg alloys. In the T5 heat treatment, nano-scale Mg_2Si precipitates are formed and can act as obstacles to dislocation movement during deformation, leading to a higher $R_{P0.2}$ [17]. Under the T51 condition which simulates the automotive paint baking process, averaged $R_{P0.2}$ increases from 113.7 MPa for the as-cast AlSiCr alloy to 142.1 MPa and 175.0 MPa for the AlSiCr0.2Mg alloy and AlSiCr0.3Mg alloy, respectively. The AlSiCr0.3Mg alloy shows a much stronger response to T51 treatment, due to a higher Mg supersaturation in the α-Al matrix after solidification. Under the T52 condition, averaged $R_{P0.2}$ increases significantly to 182.6 MPa and 212.0 MPa for the AlSiCr0.2Mg alloy and AlSiCr0.3Mg alloy, respectively. In the meantime, averaged EL is reduced from 15.1% to 7.7% and 7.4% accordingly. It is worth noting that the EL of the AlSiCr0.3Mg alloy is very close to that of the AlSiCr0.2Mg alloy, irrespective of temper, though the former has a considerably higher $R_{P0.2}$. According to Fig. 4(b), the T5 heat treatment shows minor impact on UTS.

Figure 5(a) shows typical etched macrostructures of the cross-sections at the location illustrated in Fig. 2 (Line A), for the Mg-free and Mg-added Al-Si-Cr alloys, under OM observation. White contrasted region indicates α-Al grains and black contrasted region indicates eutectic structures comprising α-Al grains and eutectic Si. A macro-level feature deserving notice is the dilatant shear band as arrowed in Fig. 5(a), which exhibits dark contrast due to segregation of the eutectic phase. During the filling of die cavity, shear strain localizes into regions of lower solid fraction which eventually develops into dilatant shear bands [18]. Figure 5(b) shows microstructures along the radial of tensile bars. The α-Al grains near the surface are finer. This is because that during the filling, alloy melt firstly impinges on the surface of die cavity wall and cools very

Table 3: A summary of averaged tensile properties

Alloy	State	$R_{P0.2}$ (MPa)	UTS (MPa)	EL (%)
AlSiCr	AC	113.7±5.1	251.6±1.1	15.1±1.4
AlSiCr0.2Mg	AC	127.6±0.9	281.2±1.0	13.6±1.3
	T51	142.1±1.8	276.0±1.6	12.1±0.8
	T52	182.6±2.4	286.5±1.9	7.7±1.0
AlSiCr0.3Mg	AC	143.9±1.5	297.0±1.1	13.3±1.6
	T51	175.0±1.5	299.0±1.5	11.0±0.9
	T52	212.0±2.2	307.0±1.6	7.4±0.9
AlSiCr0.5Cu	AC	112.8±1.4	276.3±0.5	14.6±0.2
	T51	113.6±2.8	278.8±2.2	13.3±1.3
	T52	112.2±2.9	268.6±2.3	12.7±0.9
AlSiCr0.2Mg0.5Cu	AC	131.6±1.3	299.0±1.7	12.8±1.7
	T51	151.1±3.2	297.8±2.3	10.4±0.4
	T52	187.9±1.9	306.3±2.6	7.0±0.6
AlSi10MnMg	AC	143.8±2.4	306.9±3.1	10.3±2.1
	T7	116.6±1.4	185.8±1.1	15.4±1.9

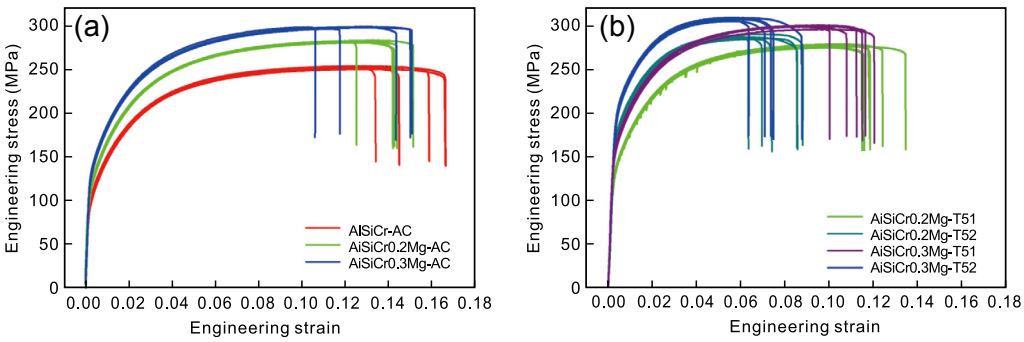

Fig. 3: Tensile stress-strain curves for Mg-free and Mg-containing Al-Si-Cr die casting alloys in as-cast (a) and T5 heat treated (b) states

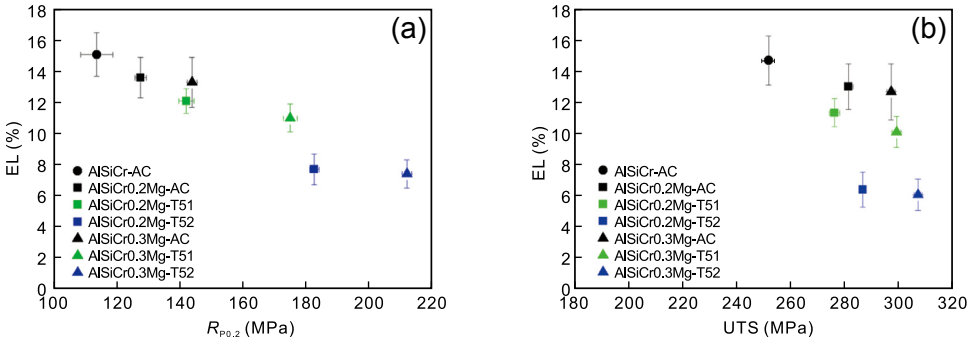

Fig. 4: Plots of 0.2% proof stress (a) and ultimate tensile stress (d) vs. elongation

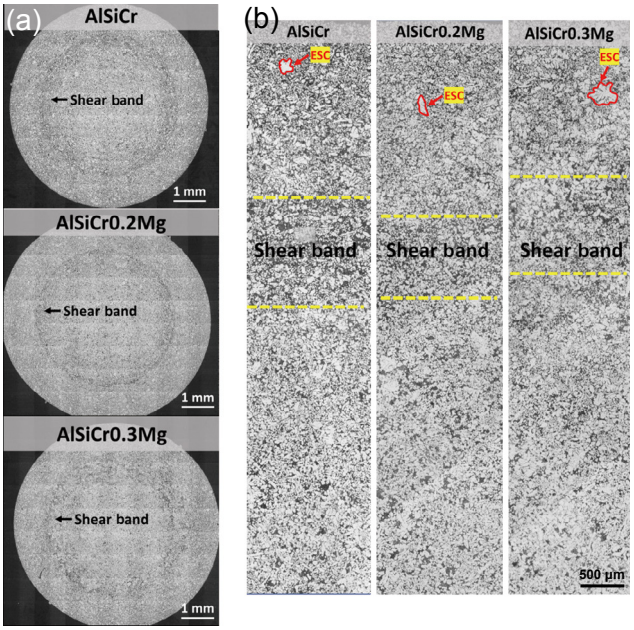

Fig. 5: Optical microscopic characterization of macrostructures of cross-sections (a) and microstructures along the radial direction (b) for Mg-free and Mg-containing Al-Si-Cr alloys

rapidly, inducing a refined microstructure [19–20]. In addition, some coarse grains are observed as those delineated by red curves in Fig. 5(b). They are primary α-Al grains crystallized in shot sleeve, and in some cases the solid fraction of pre-crystallized grains in shot sleeve can reach up to approximately 30% [8]. These α-Al grains are referred to as externally solidified crystals (ESCs) [21]. Approaching to the center, the fraction of ESCs remarkably increases. This is because the coarse ESCs enter the die cavity with the melt flow and they tend to migrate toward the center region [22]. ESCs are lean in solutes and therefore softer than the fine α-Al grains which crystallized in the die cavity. The volume fraction and distribution of ESCs, which are dependent on shot sleeve temperature, slow shot speed and melt temperature in the holding furnace, have an impact on mechanical properties [23–24]. Without strict control of casting parameters, grain size distribution in the microstructure of HPDC samples may vary shot by shot resulting in variations in tensile ductility.

Figures 6–8 show the SEM characterization results for cross-section microstructures of tensile bars along the radial direction. In the Mg-free Al-Si-Cr alloy, the detected intermetallic compounds (IMCs) mainly include primary Al-(Cr, Fe)-Si particles which were formed in shot sleeve and eutectic Al-(Cr, Fe)-Si particles which were formed in the die cavity (Fig. 6). The former is of a larger size and blocky morphology while the latter is of smaller size and irregular morphology. The volume fraction of the eutectic Al-(Cr, Fe)-Si phase appears to be much less in the center region. Mg addition leads to the formation of eutectic Al-Fe-Mg-Si phase, as shown in Figs. 7 and 8. Eutectic Al-Fe-Mg-Si phase has a weak gray contrast in the SEM secondary electron (SE) images, and can be readily identified according to the EDS mapping results. It seems that the fraction of eutectic Al-(Cr, Fe)-Si phase in the Mg-added alloys is less than that in the Mg-free alloy, especially in the near-surface region. A potential explanation is that Fe atoms in eutectic liquid are tied up in the Al-Fe-Mg-Si phase during solidification which suppress the formation of eutectic Al-(Cr, Fe)-Si phase. Eutectic Al-Fe-Mg-Si phase may be more benign to tensile ductility than the eutectic Al-(Cr, Fe)-Si phase. Therefore, Mg addition improves strength for the Al-Si-Cr alloy without significantly reducing the ductility.

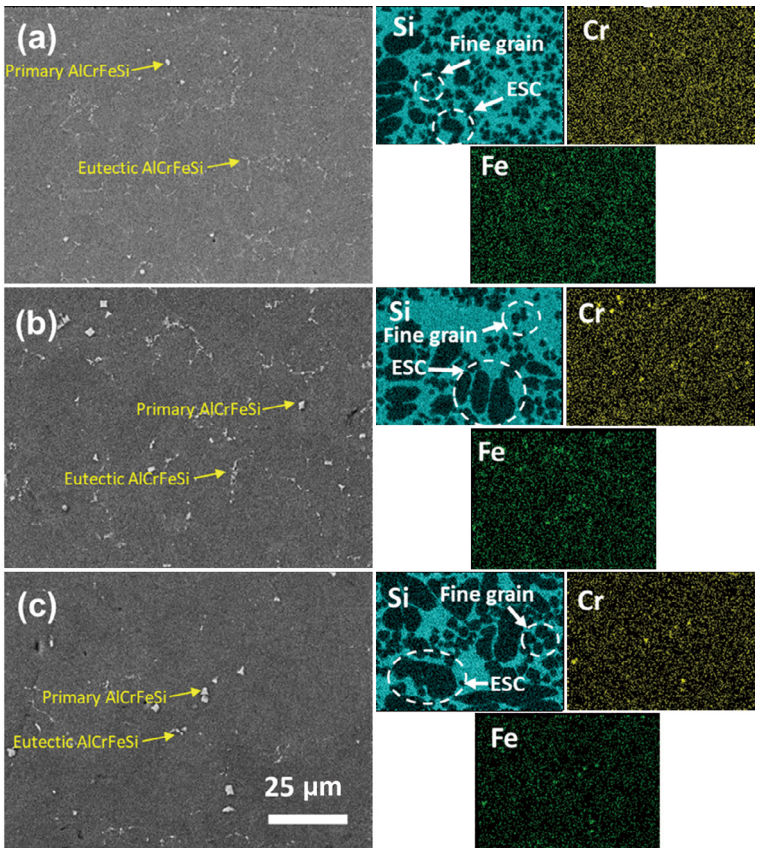

Fig. 6: SEM images (secondary electron mode) and corresponding elemental mapping from the cross-section microstructure of AlSiCr alloy: (a) region near the surface; (b) intermediate region; (c) central region

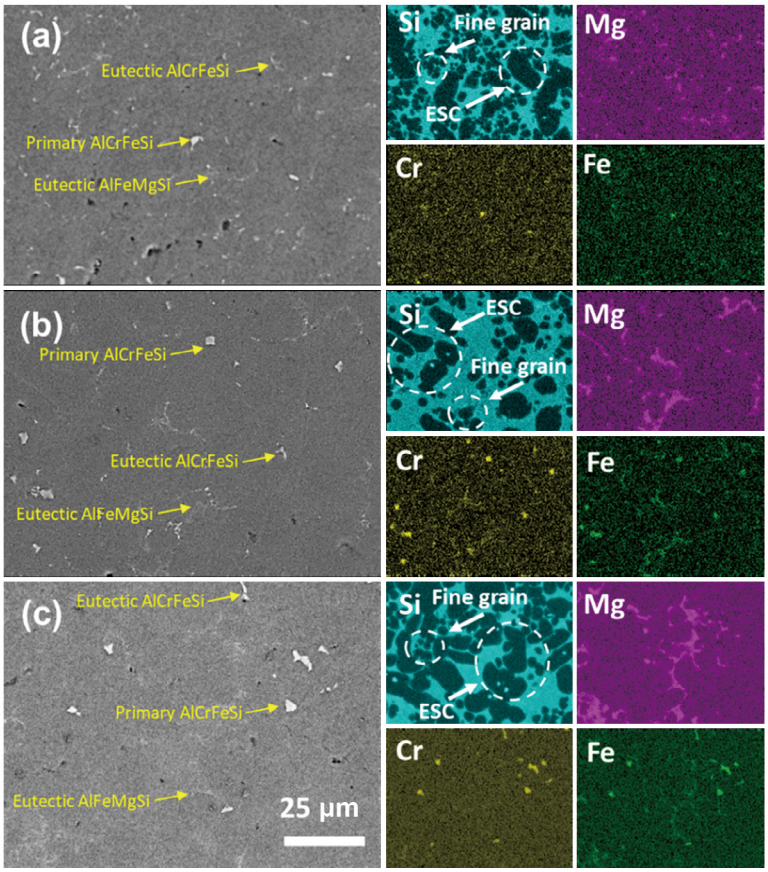

Fig. 7: SEM images (secondary electron mode) and corresponding elemental mapping from the cross-section microstructure of AlSiCr0.2Mg alloy: (a) region near the surface; (b) intermediate region; (c) central region

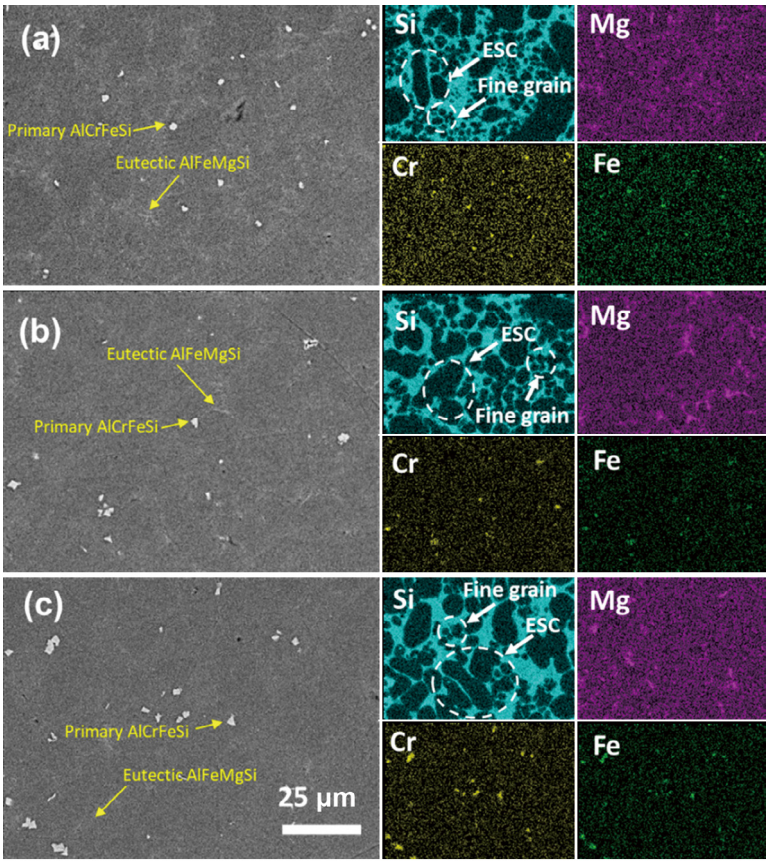

Fig. 8: SEM images (secondary electron mode) and corresponding elemental mapping from the cross-section microstructure of AlSiCr0.3Mg alloy: (a) region near the surface; (b) intermediate region; (c) central region

3.2 Effects of Cu addition on tensile properties and microstructures

Tensile curves for the Cu-free and Cu-added Al-Si-Cr die casting alloys in the AC state and T5 heat treated states are shown in Figs. 9(a) and (b), respectively. Figures 10(a) and (b) were plotted based on averaged $R_{P0.2}$, averaged UTS and averaged EL listed in Table 2 to show the impacts of Cu addition and T5 heat treatment on tensile properties. It can be seen that for the Mg-free Al-Si-Cr alloy in the AC state, 0.5wt.% Cu addition significantly enhances UTS in accompany with minor impacts on $R_{P0.2}$ and EL. According to stress-strain curves shown in Fig. 9(a), it is found that Cu addition mainly affects strain hardening capability of the Mg-free Al-Si-Cr alloy under AC condition. Solid solution strengthening from Cu atoms is probably responsible for this enhanced strain hardening rate. Under the T5 conditions, EL of the Mg-free Al-Si-Cr alloy is degraded to some extent with Cu additions. In the meantime, $R_{P0.2}$ and UTS remain similar after T5 heat treatment. During the T5 heat treatment, supersaturated Cu solution in the AC state is decomposed to form Al-Cu precipitates [25]. As the Cu addition is much lower than that in the 2xxx Al wrought alloys, the volume fraction of the obtained Al-Cu precipitate may be very limited and therefore has very minor impact on strength. For the Mg-added Al-Si-Cr alloy, 0.5wt.% Cu addition improves strength while reduces ductility accordingly, irrespective of temper [Figs. 10(a–b)]. This is because when Mg exists in the

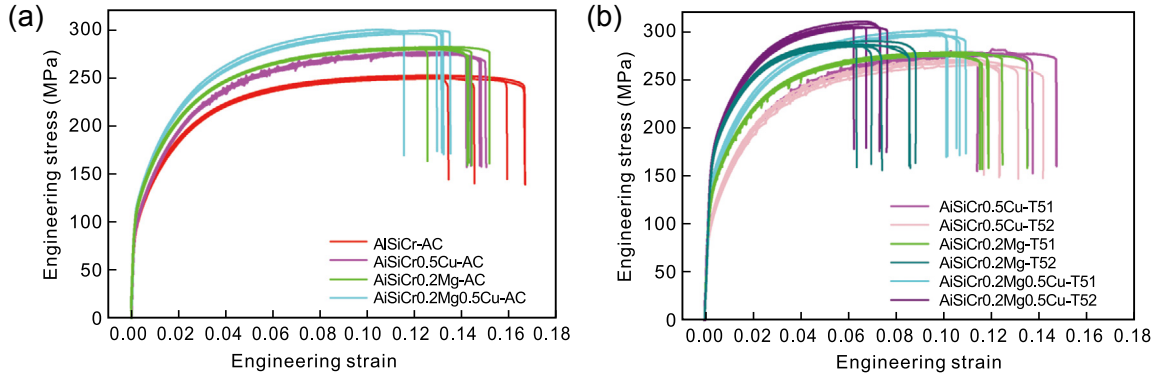

Fig. 9: Tensile stress-strain curves for Cu-free and Cu-containing Al-Si-Cr die casting alloys in as-cast (a) and T5 heat treated (b) states

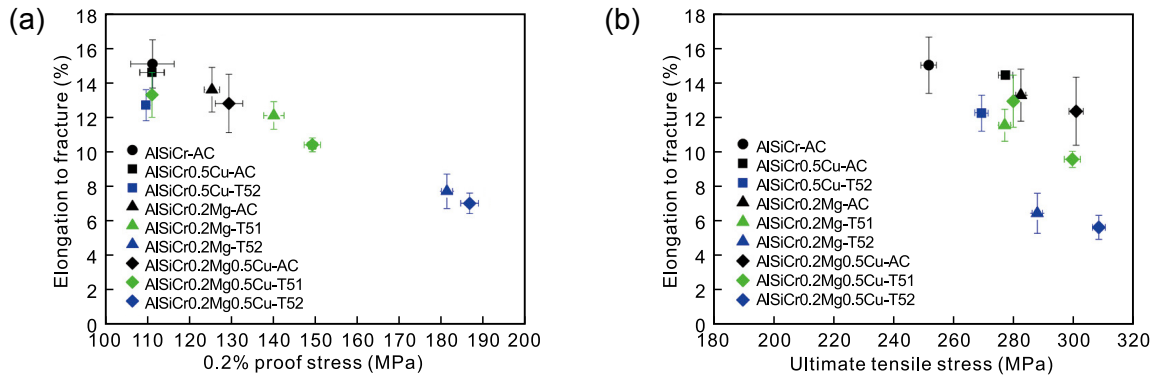

Fig. 10: Plots of 0.2% proof stress (a) and ultimate tensile stress (b) vs. elongation

alloy, Cu addition transforms ageing-induced Mg-Si precipitates to Al-Cu-Mg-Si precipitates and increases the total volume fraction of precipitates [26]. It is worth noting that for the AlSiCr0.2Mg alloy, 0.5wt.% Cu addition is still not very effective in improving $R_{P0.2}$ [Fig. 10(a)]. In contrast, increasing Mg content from 0.25wt.% to 0.39wt.% is much more effective in improving $R_{P0.2}$ [Fig. 4(a)].

Typical etched macrostructures of cross-sections of the AlSiCr0.5Cu and AlSiCr0.2Mg0.5Cu alloys are shown in Fig. 11. They have similar characteristics as described in Fig. 5. Figures 12 and 13 show SEM characterization results for the cross-section microstructures of the AlSiCr0.5Cu alloy and AlSiCr0.2Mg0.5Cu alloy, respectively. Comparing Fig. 12 to Fig. 6, adding 0.5wt.% Cu to the AlSiCr alloy induces the formation of Cu-bearing IMCs of bright contrast. These Cu-bearing IMCSs are speculated to be eutectic Al_2Cu phase which formed in the very late stage of solidification [27,28]. The slight reduction in ductility with 0.5wt.% Cu addition into the AlSiCr alloy [Fig. 10(a)] may be attributed to the formation of eutectic Al_2Cu phase which is more fragile than the Al matrix.

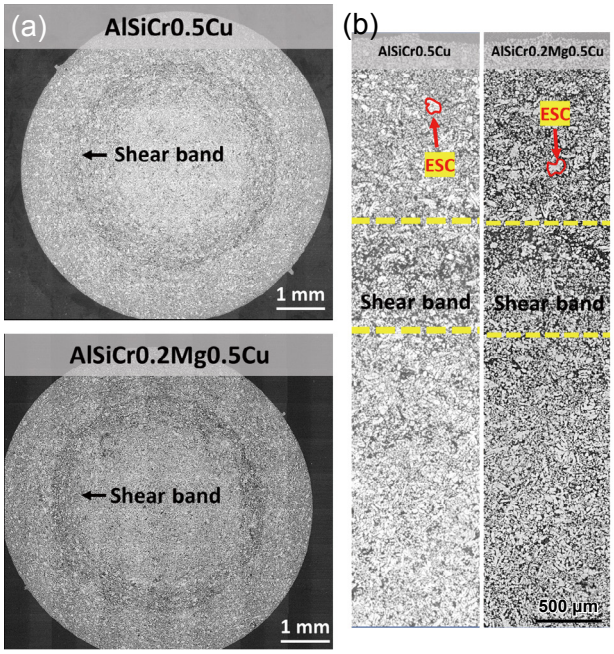

Fig. 11: Optical microscopic characterization on macrostructures of cross-sections (a) and microstructures along radial direction (b) for Cu-containing Al-Si-Cr alloys

While combined addition of Mg and Cu into Al-Si-Cr die cast alloy leads to the formation of a great amount of eutectic Al-Cu-Mg-Si IMCs in the as-cast microstructure, as shown in Fig. 13. The eutectic Al-Cu-Mg-Si IMCs are of irregular morphology and relatively coarser in the center zone [Fig. 13(c)], which may be harmful to ductility.

3.3 Comparison of Al-Si-Cr alloys with baseline AlSi10MnMg alloy

AlSi10MnMg alloy has been widely applied in the casting of body structures [3]. To accommodate self-piercing riveting with steel sheet, AlSi10MnMg alloy needs to be T7 heat treated to spherodize eutectic Si phase for significantly improving ductility and fracture toughness [4,7,8]. For comparison purpose, tensile curves for the selected Al-Si-Cr alloys and AlSi10MnMg alloy were plotted in Fig. 14(a). Figures 14(b) and (c) were plotted to show average $R_{P0.2}$, average UTS and average EL for the tensile curves in Fig. 14(a). In the AC state, AlSi10MnMg alloy shows an average $R_{P0.2}$ of 143.8 MPa and an average EL of 10.3%. In contrast, the as-cast AlSiCr0.3Mg alloy has very similar strength property but much higher ductility of 13.3% in EL. The inferior ductility of AlSi10MnMg results from its much higher silicon content. A higher silicon level is beneficial for fluidity of melt in cavity filling but results in a higher volume fraction of eutectic structure which is fragile [29-31]. After T7 heat treatment, average EL of AlSi10MnMg is improved remarkably to 15.5% but its average $R_{P0.2}$ is reduced to 116.6 MPa. In addition, strain hardening rate of T7 heat treated AlSi10MnMg alloy is much lower and UTS of T7 heat treated AlSi10MnMg is therefore reduced to only 185.8 MPa. According to Figs. 14(b, c), the average $R_{P0.2}$ (113.7 MPa) and average EL (15.1%) of the Mg-free Al-Si-Cr alloy in the AC state are comparable to the counterparts of the T7 heat treated AlSi10MnMg alloy. It is inferred that to achieve a comparable ductility as T7 heat treated AlSi10MnMg alloy, Mg and Cu additions should be minimized for Al-Si-Cr die cast alloys.

Typical etched macrostructures of cross-sections of the AlSi10MnMg alloy and the Mg-added Al-Si-Cr alloys are shown in Fig. 15. From Fig. 15(a), it is found that the width of shear band is larger in AlSi10MnMg alloy due to its higher fraction of eutectic liquid in the latest solidification stage. In addition, volume fraction of ESCs in AlSi10MnMg alloy is less than those in the Mg-added Al-Si-Cr alloys, according

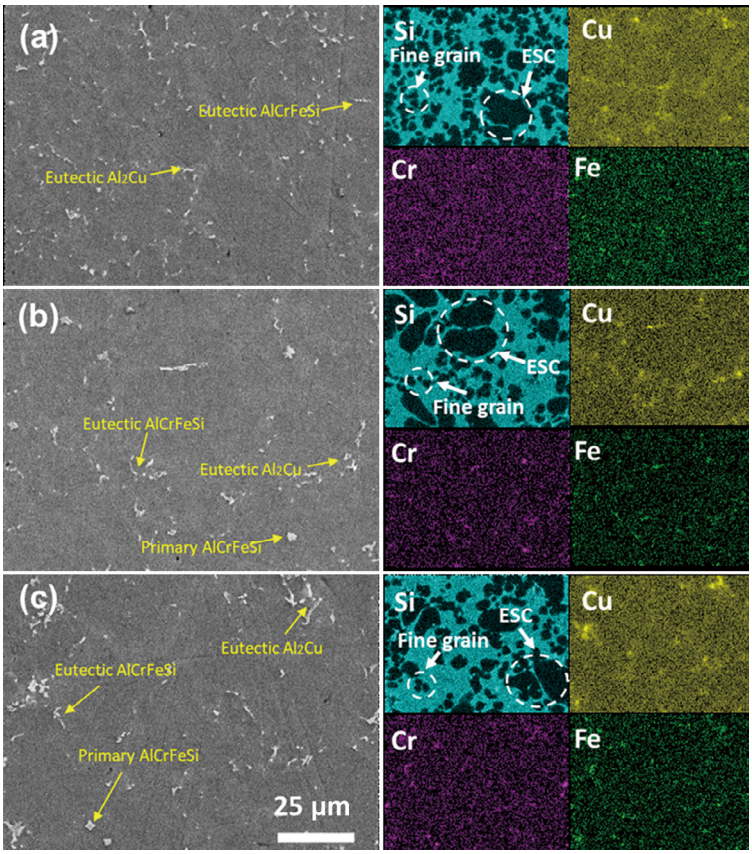

Fig. 12: SEM images (secondary electron mode) and corresponding elemental mapping of the cross-section microstructure of AlSiCr0.5Cu alloy: (a) region near the surface; (b) intermediate region; (c) central region

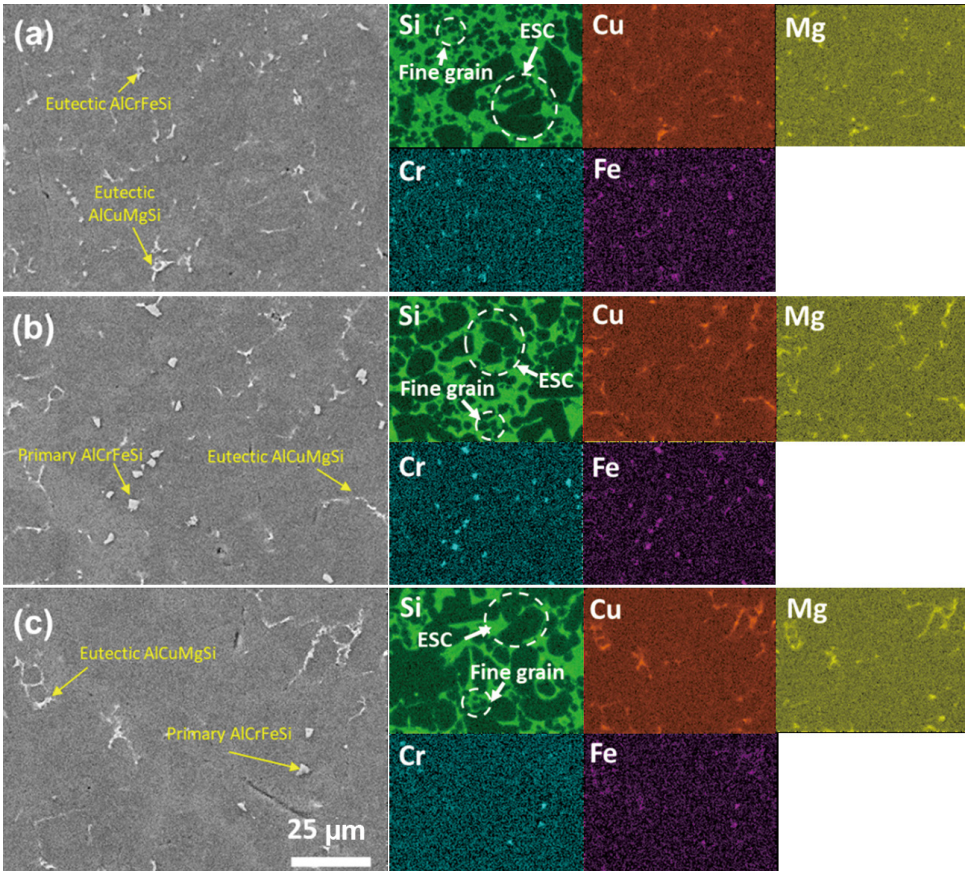

Fig. 13: SEM images (secondary electron mode) and corresponding elemental mapping of the cross-section microstructure of AlSiCr0.2Mg0.5Cu alloy: (a) region near the surface; (b) intermediate region; (c) central region

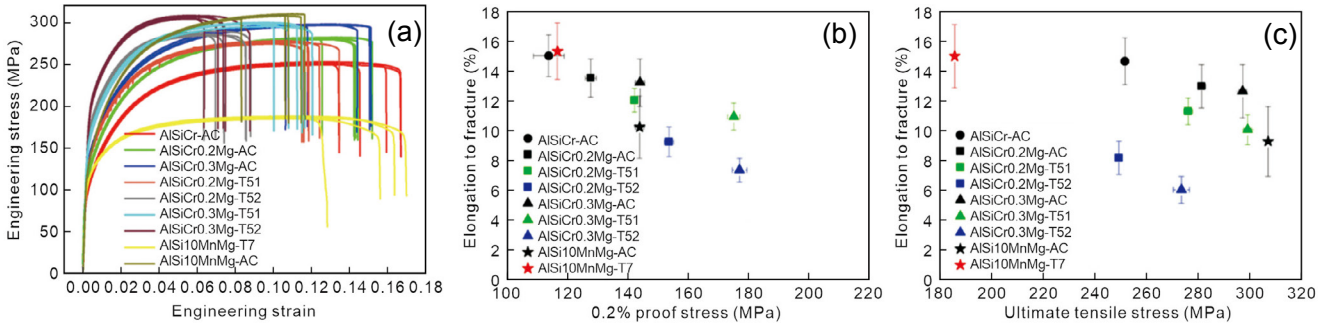

Fig. 14: Tensile stress-strain curves (a), and plots of 0.2% proof stress (b) and ultimate tensile stress (c) vs. elongation for AlSi10MnMg alloy and selected Al-Si-Cr alloys

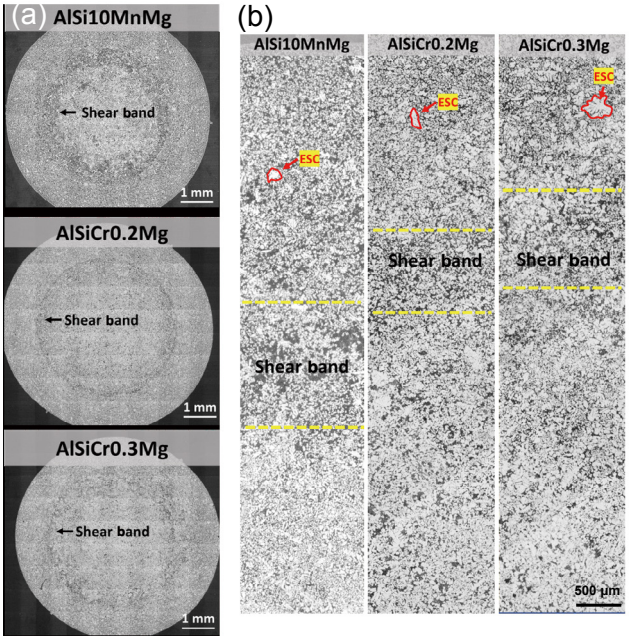

Fig. 15: Optical microscopic characterization on macrostructures of cross-sections (a) and microstructures along radius direction (b) for AlSi10MnMg alloy and Mg-added Al-Si-Cr alloys

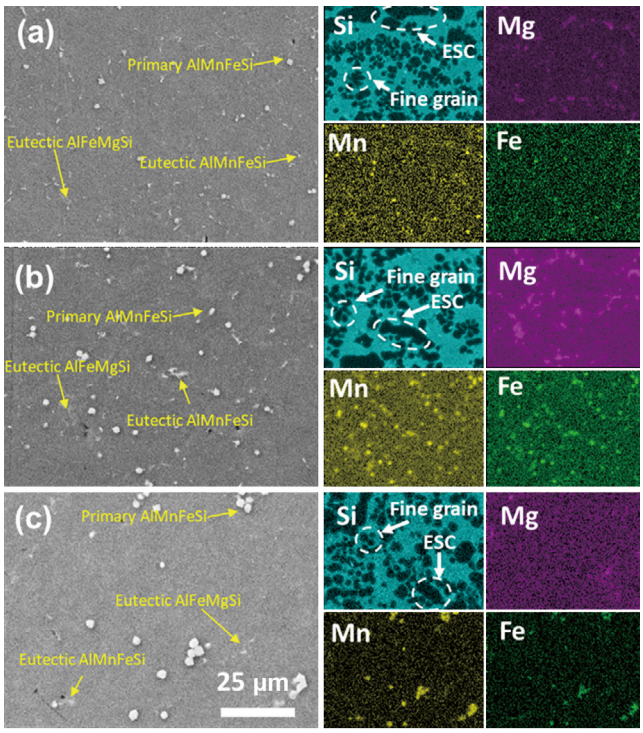

Fig. 16: SEM images (secondary electron mode) and corresponding elemental mapping of the cross-section microstructure of AlSi10MnMg alloy: (a) region near the surface; (b) intermediate region; (c) central region

to Fig. 15(b). This is because increased Si level will decrease crystallization temperature of α-Al grains, impeding the pre-crystallization of α-Al grains in shot sleeve. According to thermodynamic calculations conducted using PANDAT 2021 software with PanAl2021 database, α-Al grain starts to crystallize at 585 °C and 603 °C in Al-11.2Si-0.2Fe-0.31Mg-0.55Mn (wt.%) and Al-8.5Si-0.2Fe-0.25Mg-0.3Cr (wt.%) systems, respectively. It is therefore speculated that when the alloy melt is poured into shot sleeve with the same melt temperature and heat loss, more ESCs formed in shot sleeve for the Al-Si-Cr alloys.

Figure 16 shows the SEM characterization results for the cross-section microstructures of the as-cast AlSi10MnMg alloy. Fe-rich IMCs in AlSi10MnMg alloy is $Al_{15}(Mn, Fe)_3Si_2$ phase, based on the previous study on the Al-Si-Mn-Mg die casting alloy [32]. Comparing Fig. 16 to Figs. 6–8, it seems that the volume of primary Fe-rich IMCs of blocky morphology is higher in AlSi10MnMg alloy. It needs to be noted that Fig. 16 and Figs. 6–8 were captured at a high magnification and may not be representative region for the overall microstructures.

4 Conclusions

(1) Mg addition effectively improves the 0.2% proof stress for Al-Si-Cr die casting alloy, especially after T5 heat treatment (an artificial ageing heat treatment conducted following shape casting). Further increase of Mg content from 0.25wt.% to 0.39wt.% induces much stronger strengthening effects while ductility is not significantly sacrificed, irrespective of tempers.

(2) Effects of Cu addition on the tensile properties of AlSiCr die casting alloy are influenced by the presence of Mg in the alloy. For the Mg-free alloy in the as-cast state, 0.5wt.% Cu addition has a minor impact on the 0.2% proof stress and tensile ductility while strain hardening rate can be greatly enhanced. After T5 heat treatment, ductility is reduced with the Cu addition. In contrast, when Mg is present in the alloy, the 0.2% proof stress is improved whereas ductility is reduced

with the Cu addition, irrespective of tempers.

(3) For the Al-Si-Cr die casting alloy in the as-cast state, to obtain tensile properties comparable to that of the T7 heat treated AlSi10MnMg alloy, Mg and Cu contents in the Al-Si-Cr alloy should be minimized. The Al-Si-Cr alloy with an approximate composition of Al-8.5wt.%Si-0.3wt.%Cr-0.2wt.%Fe in the as-cast state shows very similar tensile property as the T7 heat treated AlSi10MnMg alloy.

Acknowledgement

The authors would like to acknowledge the testing assistance from Mr. Hu Yao from the Central South University.

Conflict of interest

The authors declare that they have no conflicts.

References

[1] Du J D, Han W J, Peng Y H, et al. Potential for reducing GHG emissions and energy consumption from implementing the aluminum intensive vehicle fleet in China. Energy, 2010, 35(12): 4671–4678.
[2] Bonollo F, Gramegna N, Timelli G. High-pressure die-casting: Contradictions and challenges. JOM, 2015, 67: 901–908.
[3] Youssef M Y A. A cost-efficient process route for the mass production of thin-walled structural aluminium body castings. Doctoral Dissertation, Aachen Germany: RWTH Aachen University, 2021.
[4] Luo A A, Sachdev A K and Apelian D. Alloy development and process innovations for light metals casting. Journal of Materials Processing Technology, 2022, 117606.
[5] Mao H, Fu W, Lan J, et al. In: Proc. 2017 7th International Conference on Advanced Design and Manufacturing Engineering (ICADME 2017). Atlantis, 2017: 162–166.
[6] Beals R, Conklin J, Skszek T, et al. Aluminum high pressure vacuum die casting applications for the multi material lightweight vehicle program (MMLV) body structure. Light Metals 2015, edited by Hyland M, Springer, 2015: 215–221.
[7] Sigworth G K and Donahue R J. The metallurgy of aluminum alloys for structural high-pressure die castings. International Journal of Metalcasting, 2021, 15: 1031–1046.
[8] Liu R X, Zheng J, Godlewski L, et al. Influence of pore characteristics and eutectic particles on the tensile properties of Al-Si-Mn-Mg high pressure die casting alloy. Materials Science and Engineering: A, 2020, 783: 139280.
[9] Hu B. Aluminum alloys. US Patent No. 10927436, 2021.
[10] Niu G D, Wang J, Li J P, et al. The formation mechanism of the chill fine-grain layer with high supersaturation and its influence on the mechanical properties of die casting Al-7Si-0.5 Mg alloy. Materials Science and Engineering: A, 2022, 833: 142544.
[11] Deng X, Wang Y, Wang J, et al. Quench sensitivity of A379 alloy under high-pressure die-casting and gravity-casting processes. In: Proceedings of the Institution of Mechanical Engineers, Part L: Journal of Materials: Design and Applications, 2022, 14644207221081620.
[12] Zeren M, Karakulak E and Gümüş S. Influence of Cu addition on microstructure and hardness of near-eutectic Al-Si-*x*Cu-alloys. Transactions of Nonferrous Metals Society of China, 2011, 21: 1698–1702.
[13] Moustafa M, Samuel F, Doty H, et al. Effect of Mg and Cu additions on the microstructural characteristics and tensile properties of Sr-modified Al-Si eutectic alloys. International Journal of Cast Metals Research, 2002, 14: 235–253.
[14] Sjölander E and Seifeddine S. The heat treatment of Al-Si-Cu-Mg casting alloys. Journal of Materials Processing Technology, 2010, 210: 1249–1259.
[15] Yang Y, Yu K L, Li Y G, et al. Evolution of nickel-rich phases in Al-Si-Cu-Ni-Mg piston alloys with different Cu additions. Materials & Design, 2012, 33: 220–225.
[16] Yıldırım M and Özyürek D. The effects of Mg amount on the microstructure and mechanical properties of Al-Si-Mg alloys. Materials & Design, 2013, 51: 767–774.
[17] Murayama M and Hono K. Pre-precipitate clusters and precipitation processes in Al-Mg-Si alloys. Acta Materialia, 1999, 47: 1537–1548.
[18] Gourlay C, Laukli H and Dahle A. Defect band characteristics in Mg-Al and Al-Si high-pressure die castings. Metallurgical and Materials Transactions: A, 2007, 38: 1833–1844.
[19] Dahle A, Sannes S, John D S, et al. Formation of defect bands in high pressure die cast magnesium alloys. Journal of Light Metals, 2001, 1: 99–103.
[20] Chen Z. Skin solidification during high pressure die casting of Al-11Si-2Cu-1Fe alloy. Materials Science and Engineering: A, 2003, 348: 145–153.
[21] Laukli H, Lohne O, Sannes S, et al. Grain size distribution in a complex AM60 magnesium alloy die casting. International Journal of Cast Metals Research, 2003, 16: 515–521.
[22] Gourlay C M, Dahle A K and Laukli H I. Segregation band formation in Al-Si die castings. Metallurgical and Materials Transactions: A, 2004, 35: 2881–2891.
[23] Dou K, Lordan E, Zhang Y, et al. A novel approach to optimize mechanical properties for aluminium alloy in high pressure die casting (HPDC) process combining experiment and modelling. Journal of Materials Processing Technology, 2021, 296: 117193.
[24] Jiao X Y, Zhang Y F, Wang J, et al. Characterization of externally solidified crystals in a high-pressure die-cast AlSi10MnMg alloy and their effect on porosities and mechanical properties. Journal of Materials Processing Technology, 2021, 298: 117299.
[25] Vaithyanathan V, Wolverton C and Chen L. Multiscale modeling of θ′ precipitation in Al-Cu binary alloys. Acta Materialia, 2004, 52: 2973–2987.
[26] Chakrabarti D and Laughlin D E. Phase relations and precipitation in Al-Mg-Si alloys with Cu additions. Progress in Materials Science, 2004, 49: 389–410.
[27] Samuel A, Gauthier J and Samuel F. Microstructural aspects of the dissolution and melting of Al_2Cu phase in Al-Si alloys during solution heat treatment. Metallurgical and Materials Transactions: A, 1996, 27: 1785–1798.
[28] Li Z, Samuel A, Samuel F, et al. Effect of alloying elements on the segregation and dissolution of $CuAl_2$ phase in Al-Si-Cu 319 alloys. Journal of Materials Science, 2003, 38: 1203–1218.
[29] Joseph S and Kumar S. A systematic investigation of fracture mechanisms in Al-Si based eutectic alloy – Effect of Si modification. Materials Science and Engineering: A, 2013, 588: 111–124.
[30] Guiglionda G and Poole W J. The role of damage on the deformation and fracture of Al-Si eutectic alloys. Materials Science and Engineering: A, 2002, 336: 159–169.
[31] Hafiz M and Kobayashi T. Fracture toughness of eutectic Al-Si casting alloy with different microstructural features. Journal of Materials Science, 1996, 31: 6195–6200.
[32] Jiao X Y, Liu C F, Zuo Z P, et al. The characterization of Fe-rich phases in a high-pressure die cast hypoeutectic aluminum-silicon alloy. Journal of Materials Science & Technology, 2020, 51(1): 54–62.